Physics Letters A 377 (2013) 1814–1821

Contents lists available at SciVerse ScienceDirect

Physics Letters A

www.elsevier.com/locate/pla

Dynamical properties for an ensemble of classical particles moving in a driven potential well with different time perturbation

Diogo Ricardo da Costa [a,b,*], I.L. Caldas [a], Edson D. Leonel [c]

[a] Instituto de Física, Universidade de São Paulo, Rua do Matão, Cidade Universitária, 05314-970 São Paulo, SP, Brazil
[b] School of Mathematics, University of Bristol, Bristol BS8 1TW, United Kingdom
[c] Departamento de Física, UNESP – Universidade Estadual Paulista, Av. 24A, 1515, 13506-900 Rio Claro, SP, Brazil

ARTICLE INFO

Article history:
Received 14 January 2013
Received in revised form 30 April 2013
Accepted 21 May 2013
Available online 25 May 2013
Communicated by A.R. Bishop

Keywords:
Chaos
Two-dimensional mapping
Dynamical system
Potential well

ABSTRACT

We consider dynamical properties for an ensemble of classical particles confined to an infinite box of potential and containing a time-dependent potential well described by different nonlinear functions. For smooth functions, the phase space contains chaotic trajectories, periodic islands and invariant spanning curves preventing the unlimited particle diffusion along the energy axis. Average properties of the chaotic sea are characterised as a function of the control parameters and exponents describing their behaviour show no dependence on the perturbation functions. Given invariant spanning curves are present in the phase space, a sticky region was observed and show to modify locally the diffusion of the particles.

1. Introduction

After the seminal paper of Buttiker and Landauer [1] dealing with the tunnelling through a time-dependent barrier, many results on this thematic have been reported. Among them it is interesting to mention a drift of particles at a sequence of 1D time-dependent potential wells [2] and the investigation of the dwell time for a classical particle confined to move in a periodically time varying potential well [3,4]. Periodically modulated quantum channel was also used to study quantised ballistic conductance [5], transport properties for GaAs/AlGaAs were considered [6,7], while an intense electric field was used to characterise quantum transport in semiconductors super-lattices and multiple quantum wells [8]. More rigorous and analytical investigations were made for a two-level system [9,10] particularly using Laplace transform to obtain the probability of a particle to be transmitted from one and two barriers [11,12] while Fokker–Planck equation was applied to obtain the transition probability from one potential to the other and considering different scaling times as well as different noise lengths [13]. Applications of the formalism were also proved to be useful in a washboard potential [14] as well as in a double well potential [15]. The occurrence of phonon assisted resonance tunnelling was measured in [16] while escape time from a fluctuating barrier considering either dichotomic and Gaussian perturbations was obtained [17].

Recent applications involving Bose–Einstein Condensates (BEC) can also be discussed in this approach. A nonlinear effect which includes self-trapping in a double well potential was discussed in [18]. A modification of a double potential well which includes a barrier in the middle was used to describe a resonator [19]. Using the transfer-matrix technique, it was proved [20] that a time-dependence of the potential wells affect electron probability transmission. Heun confluent functions were used to represent the solutions of a family of double-well potential [21]. The effect of spin–orbit coupling in the tunnelling from wells in a BEC in a double well potential was discussed in [22] while a quantum phase transition in a BEC was also characterised [23]. The probability of finding a particle in a two-well periodic potential was obtained analytically in [24] while a power law was obtained in the characterisation of the survival probability of an ensemble of particles escaping from one well to the other one due to white noise [25].

In this Letter we use the same general procedure as made in [26,27] to obtain and characterise some dynamical properties for an ensemble of non-interacting (classical) particles confined to move inside of a periodically time-dependent potential well. We are seeking to understand the influence of the position of the lowest energy invariant spanning curve in the average properties of the chaotic sea. The Hamiltonian that describes the system is given by $H(x,p,t) = p^2/(2m) + V(x,t)$ where x, p and t correspond to the position, momentum coordinates and time respectively. As we

* Corresponding author at: Instituto de Física, Universidade de São Paulo, Rua do Matão, Cidade Universitária, 05314-970 São Paulo, SP, Brazil. Tel.: +55 19 3526 9174; fax: +55 19 3526 9179.
E-mail address: drcosta@usp.br (D.R. da Costa).

0375-9601/$ – see front matter
http://dx.doi.org/10.1016/j.physleta.2013.05.050

shall see in the next section, the potential $V(x,t)$ is controlled by three relevant dimensionless control parameters. If one of the control parameters is equal to zero, the system is integrable. For the other situations, the phase space of the model is of mixed type. It contains periodic islands surrounded by a chaotic sea (which is characterised by a positive Lyapunov exponent). The *size* of the chaotic sea depends on the control parameters and is limited by a set of invariant spanning curves, which prevent the unlimited energy growth of the particle. Our main goal in this Letter is to understand and describe how the shape of the periodic potential influences the dynamics of an ensemble of particles moving along the chaotic sea by the position of the lowest energy invariant spanning curve. Considering different types of perturbations, we study the behaviour of the Lyapunov exponents and some average properties of the chaotic sea including the behaviour of the deviation around the average energy. We show that critical exponents used in the scaling theory, are independent of the perturbation function proposed. We also observe a region of strong trapping regime which affects the transport along the chaotic sea.

The Letter is organised as follows. In Section 2 we describe the model and obtain the equations of the mapping. The numerical results are considered in Section 3 and final remarks and conclusions are drawn in Section 4.

2. The model and the map

In this section we discuss all the details needed to construct the mapping that describes the dynamics of the model. The system under consideration has a dynamics governed by a Hamiltonian of the type $H(x,p,t) = p^2/(2m) + V(x,t)$ where x, p and t correspond to position, momentum coordinates and time respectively.

We emphasise that different kinds of potential shape lead to similar dynamics. For a chain of infinitely many and symmetric oscillating square wells with their bottoms moving periodically and synchronised in time (see Ref. [26] and Fig. 1(a)), the dynamics leads to diffusion in space [3,4]. One can also assume a single oscillating square well with periodic boundary conditions, as shown in Fig. 1(b). Finally, a step potential whose bottom moves periodically in time confined in an infinite box of potential (see Fig. 1(c)) leads to similar results in the phase space. This last shape is used in our simulations, where the potential $V(x,t)$ is given by

$$V(x,t) = \begin{cases} \infty, & \text{if } x \leqslant 0 \text{ or } x \geqslant (a+b)/2, \\ V_0, & \text{if } 0 < x < \frac{b}{2}, \\ V_1 f(t), & \text{if } \frac{b}{2} \leqslant x < \frac{a+b}{2}, \end{cases} \tag{1}$$

where a, b, V_0, V_1 and w are the control parameters. The function $f = f(t)$ is time-dependent. Possible allusions of the time-dependent potential can be made as corresponding to the potential created by atoms localised in sequence along an infinite and symmetric chain while the oscillations may denote phonon effects or either the contact of the chain with a thermal bath. Hence the potential well is getting energy from a thermal bath and is transferring it to the particle. It is important to emphasise that the potential well considered in this Letter can indeed trap temporarily particles, see applications of trapping in a quantum dot in Ref. [28]. The shape of the phase space is strongly dependent on f. For a random perturbation, the particle exhibits unlimited diffusion in energy. On the other hand, for a smooth and periodic f the phase space is mixed. The existence of invariant spanning curves prevent the particle to exhibits unlimited energy growth. They indeed work as a physical barrier not letting the particle to pass through. The chaotic properties of the phase space are directly dependent on the location of the lowest energy invariant spanning curve and how it behaves as a function of the control parameters.

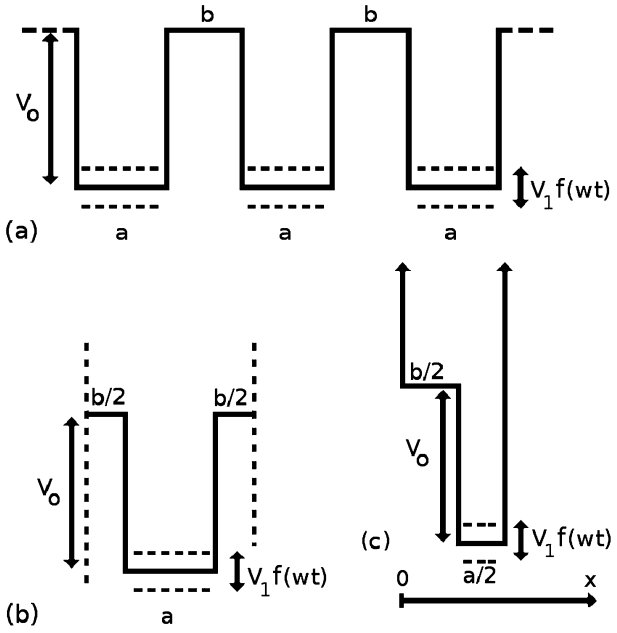

Fig. 1. Sketch of: (a) a chain of infinitely many and symmetric oscillating square wells with their bottoms moving periodically and synchronised in time. (b) A single oscillating square well. (c) A step potential whose bottom moves periodically in time.

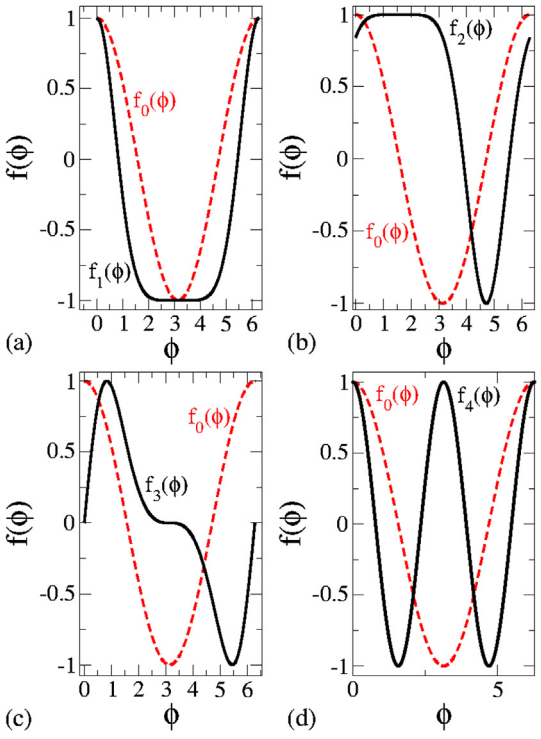

Fig. 2. (Colour online.) Plots of the functions: (a) $f_1(\phi)$; (b) $f_2(\phi)$; (c) $f_3(\phi)$; (d) $f_4(\phi)$ using $q = 2$. The dashed red lines correspond to plots for $f_0(\phi)$, used as comparison.

In this Letter we consider different expressions for $f(t)$ as shown in Fig. 2(a)–(d). The functions $f_1(\phi)$, $f_2(\phi)$, $f_3(\phi)$ and $f_4(\phi)$ are given by

$$f_1(\phi) = \cos\big[\phi + \sin(\phi)\big], \qquad f_2(\phi) = \sin\big[\phi + \cos(\phi)\big], \tag{2}$$

and

$$f_3(\phi) = \sin\big[\phi + \sin(\phi)\big], \qquad f_4(\phi) = \cos(q\phi). \tag{3}$$

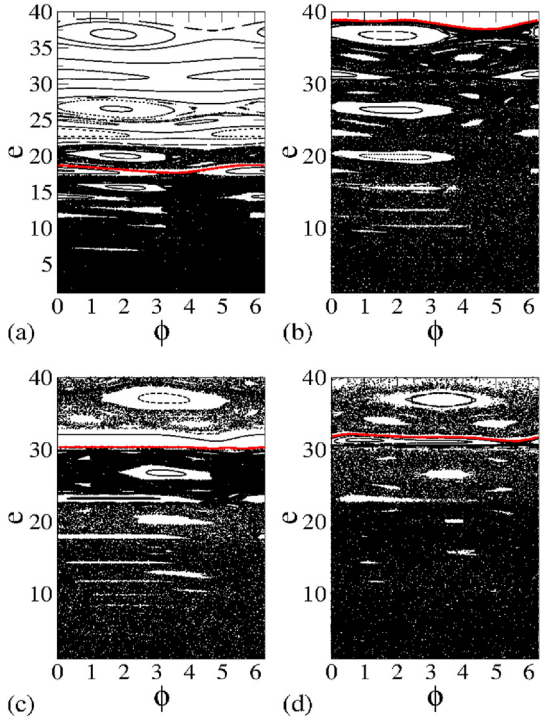

Fig. 3. (Colour online.) Plot of the phase space for mapping (4) using the control parameters $N_c = 33.18$, $r = 1$ and $\delta = 0.5$ for: (a) $f_0(\phi)$, (b) $f_1(\phi)$, (c) $f_2(\phi)$ and (d) $f_3(\phi)$. The red lines denote the position of the lowest invariant spanning curve.

where q is a positive integer number. For $q = 1$ function $f_0(\phi) = \cos[\phi]$. Results obtained for the dynamics of the particle considering function $f_4(\phi)$ are shown in the last part of this Letter.

To precisely describe the dynamics of the particle, we construct a nonlinear mapping for the variables energy of the particle and time that the particle enters the oscillating potential well. We used a procedure similar to the one discussed in Ref. [26]. We define dimensionless variables $\delta = V_1/V_0$, $r = b/a$, $e_n = E_n/V_0$, $\phi = wt$ and $N_c = w/(2\pi)$ $(a/\sqrt{2V_0/m})$. The last variable measures the time in terms of the number of oscillations of the moving well. It indeed corresponds to the number of oscillations that the potential well completes in a time $t = a/\sqrt{2V_0/m}$ for a particle moving the distance a with constant kinetic energy $K = V_0$. The mapping is written as

$$T: \quad \begin{cases} e_{n+1} = e_n + \delta[f_j(\phi_n + i\Delta\phi_a) - f_j(\phi_n)], \\ \phi_{n+1} = [\phi_n + i\Delta\phi_a + \Delta\phi_b] \bmod(2\pi), \end{cases} \tag{4}$$

where j specifies the type of function ($j = 0, \ldots, 4$ as discussed above) and i is the smallest integer number that matches the condition $e_n + \delta[f_j(\phi_n + i\Delta\phi_a) - f_j(\phi_n)] > 1$. The auxiliary variables are given by

$$\Delta\phi_a = \frac{2\pi N_c}{\sqrt{e_n - \delta f_j(\phi_n)}}, \qquad \Delta\phi_b = \frac{2\pi N_c r}{\sqrt{e_{n+1} - 1}},$$

where $\Delta\phi_a$ and $\Delta\phi_b$ represent, the time (in dimensionless variables) spend for the particle to travel the distance a and b, respectively. The phase space for mapping (4) is shown in Fig. 3(a)–(d) for different types of external perturbations and considering as fixed the parameters $N_c = 33.18$, $r = 1$ and $\delta = 0.5$. One sees that the phase space for all functions is of mixed type. When the function f_j is changed, a deformation of some KAM islands is observed and the position of the fixed points changes too. The position of the lowest invariant spanning curve depends on the function under consideration.

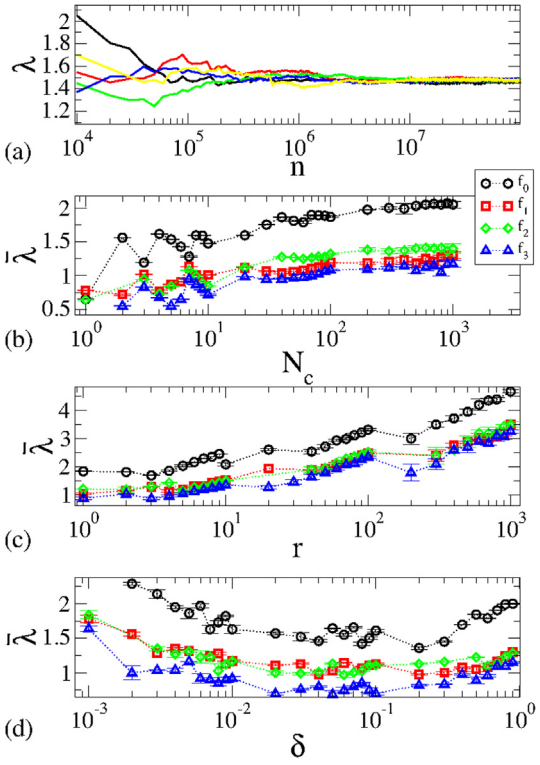

Fig. 4. (Colour online.) (a) Plot of the Lyapunov exponent as a function of n for five different initial conditions and considering the function f_0. The parameters used were $N_c = 10$, $r = 1$ and $\delta = 0.5$. For the functions f_0, f_1, f_2 and f_3 we have: (b) $\bar{\lambda}$ vs N_c for fixed $r = 1$ and $\delta = 0.5$; (c) $\bar{\lambda}$ vs r for fixed $N_c = 33.18$ and $\delta = 0.5$; (d) $\bar{\lambda}$ vs δ for fixed $N_c = 33.18$ and $r = 1$.

3. Numerical results

Let us start discussing the behaviour of the Lyapunov exponent. They are obtained as

$$\lambda_k = \lim_{n\to\infty} \frac{1}{n} \ln\left|\Lambda_k^{(n)}\right|, \quad k = 1, 2, \tag{5}$$

where $\Lambda_k{}^{(n)}$ are the eigenvalues of the matrix $M = \prod_i^n J_i(e_i, \phi_i)$ and J is the Jacobian matrix. Fig. 4(a) shows a plot of λ vs n for f_0 and considering four different initial conditions where ϕ_0 is randomly chosen in $\phi_0 \in (0, 2\pi]$ for the parameters $N_c = 10$, $r = 1$ and $\delta = 0.5$. The initial energy used was $e_0 = 1.001$. We see that after an initial fluctuation, the positive Lyapunov exponent converges to a constant value for large enough n and the saturation point depends on the values of the control parameters. The average Lyapunov exponent is given by

$$\bar{\lambda} = \frac{\sum_{i=1}^{N} \lambda_i}{N}, \tag{6}$$

where λ_i is obtained as the asymptotic behaviour for chaotic orbits considering different initial conditions. In our simulations we consider $N = 5$ and iterate the mapping up to 10^8 times for each orbit. Larger values of N produce a slight decrease of the error bars. In Fig. 4(b)–(d) we have respectively the plots of $\bar{\lambda}$ as a function of N_c, r and δ for f_0, f_1, f_2 and f_3. From Fig. 4(b), one sees that the positive Lyapunov exponent varies from $\bar{\lambda} \approx 0.5$ for $N_c = 1$ up to $\bar{\lambda} \approx 2$ for $N_c = 10^3$. It also has a monotonic tendency of growth as a function of N_c for all f_j ($j = 0, \ldots, 3$). Note however that increasing N_c corresponds to raising the number of oscillations of the well and consequently increasing the randomness of the system, therefore leading to an increase in the Lyapunov exponent. Fig. 4(c) shows a plot of $\bar{\lambda}$ vs r for fixed $\delta = 0.5$ and $N_c = 33.18$

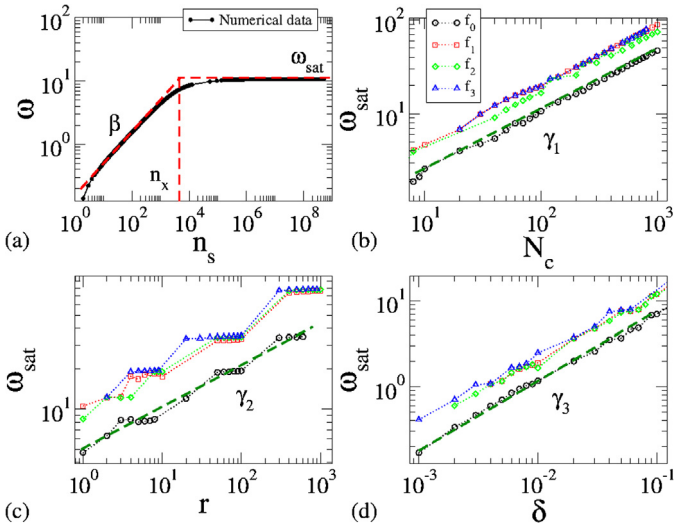

Fig. 5. (Colour online.) Plot of: (a) ω vs n using f_0 considering $N_c = 100$, $r = 1$ and $\delta = 0.5$. For functions f_0, f_1, f_2 and f_3 we have: (b) ω_{sat} vs N_c for fixed values of $r = 1$ and $\delta = 0.5$; (c) ω_{sat} vs r for fixed values of $N_c = 33.18$ and $\delta = 0.5$; (d) ω_{sat} vs δ for fixed values of $N_c = 300$ and $r = 1$. Numerical values for critical exponent are shown in Table 2.

and different functions f_j. Increasing r for a fixed N_c and δ corresponds to enlarge b thus increasing the distance from the well up to the box of potential. Such an increase leads to a long flight of the particle until next entrance in the oscillating square well therefore yielding an increase of the number of oscillations of the moving well and consequently increasing also the randomness of the system. The sudden jumps in the behaviour of the Lyapunov exponent are explained as the destruction of invariant spanning curves leading to a joint of different chaotic regions. More details are shown in Section 3.3. Finally a plot of $\bar{\lambda}$ vs δ is shown in Fig. 4(d). The control parameters used were $r = 1$ and $N_c = 33.18$. One sees that for small values of δ, which correspond to very small fluctuations of the oscillating square well, produce a large Lyapunov exponent. A minimum value of $\bar{\lambda}$ vs δ for all f_j was observed for $\delta \approx 0.1$.

3.1. Deviation of the average energy along the low energy chaotic sea

We now discuss the behaviour of the deviation of the average energy for a chaotic orbit in the regime of low energy. To do so, we define the average energy as

$$\bar{e}(n, \delta, N_c, r) = \frac{1}{n}\sum_{i=1}^{n} e_i, \tag{7}$$

and hence the deviation of the average energy is written as

$$\omega(n, \delta, N_c, r) = \frac{1}{M}\sum_{j=1}^{M}\sqrt{\overline{e_j^2}(n, \delta, N_c, r) - \overline{e_j}^2(n, \delta, N_c, r)}, \tag{8}$$

where M denotes an ensemble of different initial conditions.

Fig. 5(a) shows a plot of ω vs n for $N_c = 100$, $r = 1$, $\delta_r = 0.5$ and considering function f_0. We see that ω grows as a power law for small n and with slope $\beta \approx 0.5$ and, after a crossover number n_x, ω tends to a regime of saturation reaching ω_{sat} for large enough n. A variation on the parameters N_c, r and δ produce similar plots but with different crossovers and different saturations. Therefore we propose that

(i) For $n \ll n_x$, the behaviour of ω can be described as

$$\omega\left(n\delta^2, N_c, r, \delta\right) \propto \left[n\delta^2\right]^{\beta}, \tag{9}$$

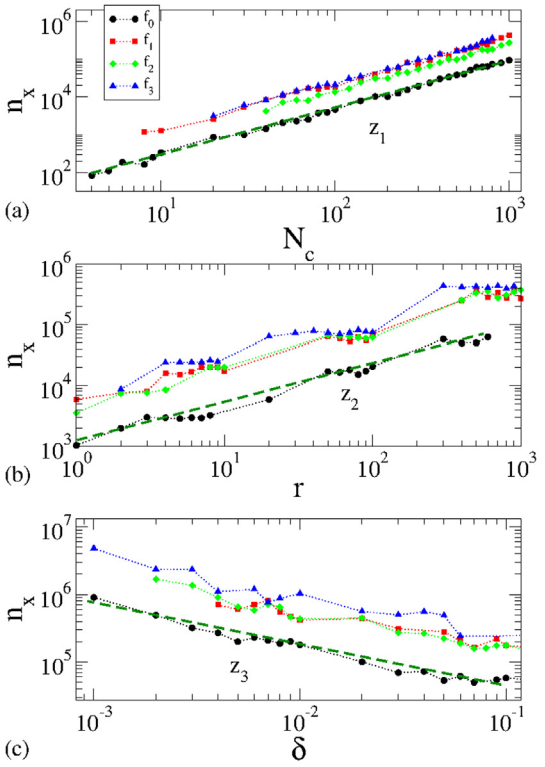

Fig. 6. (Colour online.) Plot of the crossover n_x as a function of the control parameters, considering the different functions f_0, f_1, f_2 and f_3 for: (a) n_x vs N_c for fixed $r = 1$ and $\delta = 0.5$; (b) n_x vs r for $N_c = 33.18$ and $\delta = 0.5$; (c) n_x vs δ for $N_c = 300$ and $r = 1$.

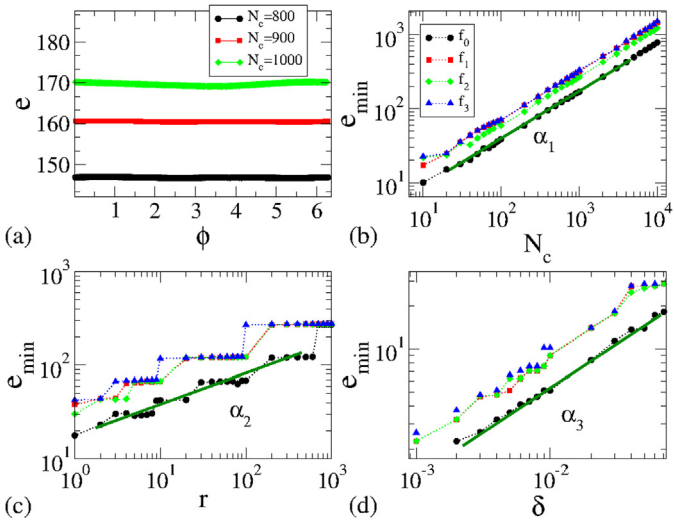

Fig. 7. (Colour online.) (a) Plot of the position of the lowest energy invariant spanning curve using the function f_0 and considering $r = 1$ and $\delta = 0.5$ for $N_c = 800$, $N_c = 900$ and $N_c = 1000$. (b) Plot of e_{min} vs N_c with corresponding slope α_1 for different functions f_i $(i = 0, 1, 2, 3)$; (c) e_{min} vs r with α_2; (d) e_{min} vs δ with slope α_3.

where β is an accelerating exponent. After extensive simulations we obtain $\beta \cong 1/2$;

(ii) For $n \gg n_x$, ω_{sat} is given by

$$\omega_{\text{sat}}\left(n\delta^2, N_c, r, \delta\right) \propto N_c^{\alpha_1} r^{\alpha_2} \delta^{\alpha_3}, \tag{10}$$

where α_1, α_2 and α_3 are critical exponents;

(iii) The characteristic crossover n_x is written as

$$n_x\left(n\delta^2, N_c, r, \delta\right) \propto N_c^{z_1} r^{z_2} \delta^{z_3}, \tag{11}$$

where z_1, z_2 and z_3 are also critical exponents.

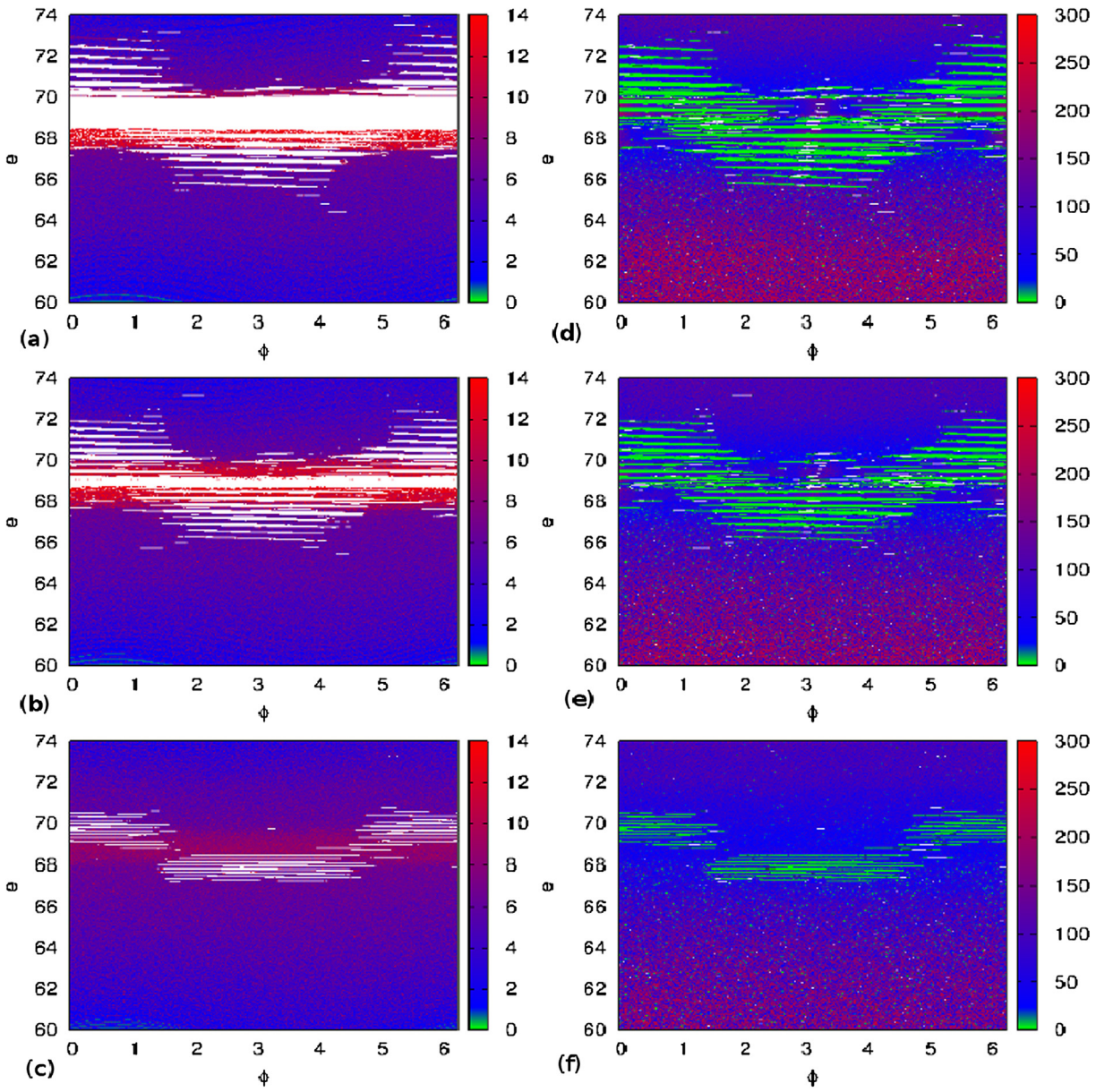

Fig. 8. (Colour online.) Grid of different initial conditions (ϕ_0, e_0) showing in colour the logarithm of the escape time (LET) for: (a) $r = 80$; (b) $r = 100$; (c) $r = 200$. Number of different return times (NDRT) for: (d) $r = 80$; (e) $r = 100$; (f) $r = 200$. The escape windows are situated at $e_1 < 59$ and $e_1 > 75$. The function F_0 was used to obtain the results.

Table 1
Critical exponents obtained analysing the deviation of the average energy.

	f_0	f_1	f_2	f_3
α_1	0.659(4)	0.651(3)	0.66(2)	0.649(6)
α_2	0.32(1)	0.30(1)	0.331(9)	0.30(1)
α_3	0.78(1)	0.76(1)	0.725(8)	0.74(2)
z_1	1.31(2)	1.30(3)	1.26(2)	1.28(2)
z_2	0.64(2)	0.61(2)	0.66(2)	0.62(3)
z_3	−0.65(3)	−0.55(4)	−0.59(2)	−0.59(6)

The exponents can be found if the behaviour of ω_{sat} and n_x are obtained as a function of the control parameters. In Fig 5(b) we have a plot of ω_{sat} vs N_c. Applying a power law fitting we found for the critical exponent α_i with $i = 1, 2, 3$, as shown in Table 1, for f_0, f_1, f_2 and f_3. Making similar procedure but varying the parameters r and δ (see Fig. 5(c) and Fig. 5(d)) we found $\alpha_2 \approx 1/3$ and α_3 as shown in Table 1.

Table 2
Exponents obtained by the lowest energy along the invariant spanning curve.

	f_0	f_1	f_2	f_3
α_1	0.657(1)	0.657(1)	0.645(4)	0.661(2)
α_2	0.37(2)	0.31(3)	0.33(1)	0.29(2)
α_3	0.64(1)	0.66(2)	0.660(9)	0.64(2)

The behaviour of the crossover n_x can be characterised as a function of the control parameters too. From Fig. 6(a), (b), (c) and applying a power law fitting we obtain for each function (f_0, f_1, f_2 and f_3) the exponents z_1, z_2 and finally z_3, as shown in Table 1.

3.2. Localisation of the lowest energy invariant spanning curve

Let us discuss in this section the organisation of the phase space in the light of the position of the lowest energy invariant spanning curve. It works as a physical barrier preventing the

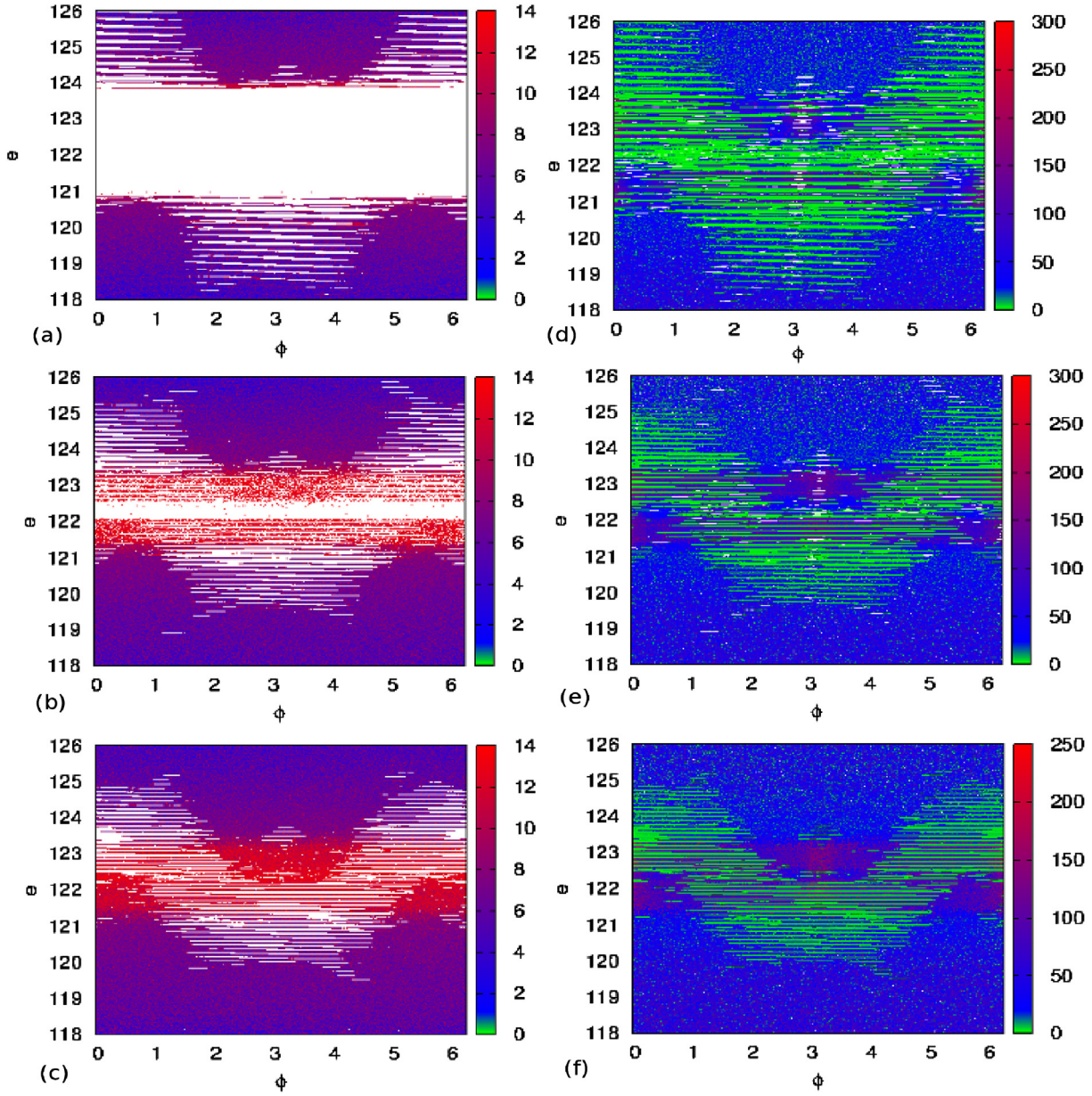

Fig. 9. (Colour online.) Grid of different initial conditions (ϕ_0, e_0) showing in colour the logarithm of the escape time (LET) for: (a) $r = 400$; (b) $r = 600$; (c) $r = 700$. Number of different return times (NDRT) for: (d) $r = 400$; (e) $r = 600$; (f) $r = 700$. The escape windows are situated at $e_1 < 117$ and $e_1 > 127$. The function F_0 was used to obtain the results.

particle to pass through. The position of the lowest one depends on the control parameters in the same way as the energy depends. Fig. 7(a) shows the localisation of the lowest energy invariant spanning curve for the parameters $r = 1$ and $\delta = 0.5$ for $N_c = 800$, $N_c = 900$ and $N_c = 1000$ considering function f_0. A plot of the lowest energy along the invariant spanning curve as a function of the parameters gives a glance of how the chaotic sea varies. Fig. 7(b) shows a plot of $e_{\min}$ vs N_c and corresponding slope α_1. Using a similar procedure, a plot of $e_{\min}$ vs r and $e_{\min}$ vs δ are shown in Fig. 7(c), (d) with their slopes also. The slopes α_1, α_2 and α_3 obtained for different functions f_0, f_1 f_2 and f_3 are shown in Table 1. We notice that the numerical values of $\alpha_1 \cong 2/3$ is remarkably well described as theoretically predicted in Ref. [29].

3.3. Behaviour of the energy as a function of the parameter r

Let us now discuss some properties of the phase space as a function of the control parameter r. As shown in Fig. 7(c), $e_{\min}$ keeps constant for certain ranges of r and then suddenly it changes. This is easily seen for the range of $r = 100$ and $r = 200$ and also for $r = 600$ and $r = 700$. In Figs. 8(a)–(f) we have grids of 10^6 equally spaced initial conditions $\phi_0 \in [0, 2\pi)$ and $e_0 \in [60, 74]$. The colours in Fig. 8(a)–(c) represent the logarithm of the escape time (LET) for each chosen initial condition. We define the escape time as the number of iterations of the mapping that the initial condition needs to escape the region in energy of $e > 75$ or $e < 59$ in Fig. 8. The maximum iteration number used was 10^6. The white colour corresponds to the region where the particle was trapped for the initial condition chosen and not escaped before 10^6 iterations. For some regions indeed the particle stays trapped forever as is the case of periodic islands. If $e > 75$ or $e < 59$, we consider that the particle escaped and another initial condition is started. As shown in Fig. 8(a) (with $r = 80$) there is a large region (white colour) where the escape time is larger than 10^6. The red colour represents the regions where stickiness is observed leading to a larger escaping time as compared to the non stickiness regions.

Such regions appear mostly near the periodic islands. The colours in Fig. 8(d)–(f) represent the number of different returning times (NDRT). To calculate them we consider a rectangle of recurrence, where each time that an orbit enters in this region a counter was accumulated and it accounts the sums of the number of different return times. For the same parameter $r = 80$ as in Fig. 8(d) we see that inside of the periodic islands, the NDRT has low values (green colour). A chaotic region is characterised by NDRT $\cong 300$ while stickiness regions are shown to have NDRT of the order of 50.

Fig. 8(b) shows the results for the LET using $r = 100$. We notice that the blank region, which represents the region where the orbits have had not access because of the stickiness, for such a parameter becomes smaller when comparing with $r = 80$. On the other hand, the results for the NDRT are approximately the same as those obtained in Fig. 8(e). If $r = 200$ and as shown in Fig. 8(c) for the analysis of the LET, we may conclude that it is possible to trespass the region with stickiness (that the blank regions disappeared), therewith the energy of the particles might grow higher. Looking at Fig. 8(f), the NDRT confirms that the sticky region becomes smaller and the islands start to disappear. Consequently the orbits reach a higher maximum of energy $e \cong 120$ as shown in Fig. 9(a) for $r = 400$. Again it is possible to observe a large blank region in the LET and consequently a large stickiness highlighted in the NDRT (see for instance Fig. 9(d)). For a larger value of r, say $r = 600$, again the blank region becomes smaller in the LET (see Fig. 9(b)), but for $r = 700$ (Fig. 9(c)) such region disappears and the energy grows higher. Same phenomenon happens for larger r and we can conclude that the plateaus of energy shown in Fig. 7(c) for $e_{\min}$ arise because of the large stickiness regions.

3.4. Results for the function $f_4(\phi)$

According to the definition of function f_4 (see Eq. (3)) for $q = 1$ function $f_0(\phi)$ is recovered. Increasing q, the number of hills and valleys increase too for a range of $\phi \in [0, 2\pi]$. Fig. 2(d) confirms this assumption for $q = 2$. Clearer an increase in q produce an increase in the randomness of the system leading the position of the lowest invariant spanning curve to rise too. Fig. 10(a) shows a plot of $e_{\min}$ vs N_c for four different values of q. As one can see, after power law fit the slopes obtained for each curve are approximately equal to 2/3. Fig. 10(b) shows a plot of $e_{\min}$ vs q. A power law fits furnishes a slope of $\alpha = 0.65557(7)$. Using such result and rescaling properly the axis in Fig. 10(a) ($e_{\min} \to e_{\min}/a^{0.65557}$) we show that the position of the lowest invariant spanning curve is scaling invariant with respect to q.

4. Summary and conclusions

We have studied the dynamics of an ensemble of classical particles confined in an infinity potential box and containing time-dependent potential wells with different perturbation functions. The square wells represented the conduction band defined by GaAs/AlGaAs [26] heterostructure or a quantum dot [26,28]. The oscillating depth in our Letter represented, for example, the electron–phonon interaction [16] or the presence of a monochromatic electromagnetic or acoustic field [7]. One of the most important results was to show that the critical exponents are independent of the perturbation function proposed for the time-dependent perturbation of the oscillating depth. It is important to say that the critical exponents describe the characteristic behaviour of a set of particles in the phase space and is controlled by the position of the lowest invariant spanning curve. The critical exponents α_i ($i = 1, 2, 3$) were obtained analysing the saturation of the deviation of the average energy as function of the control parameters. The critical exponent β was also found to be close to 1/2 for all functions f_j ($j = 0, \ldots, 4$). The critical exponent z_i ($i = 1, 2, 3$)

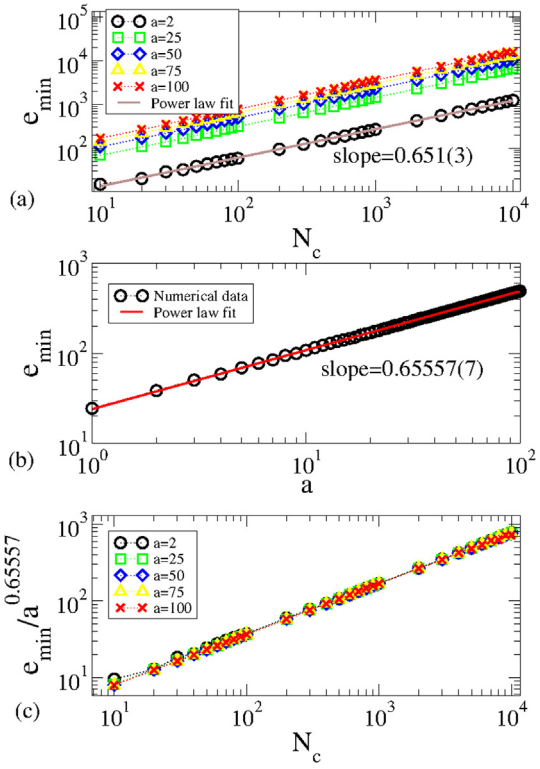

Fig. 10. (Colour online.) Plot of $e_{\min}$ vs N_c for $q = 2$, $q = 25$, $q = 50$ and $q = 100$. A power law fit gives a slope 2/3; (b) Plot of $e_{\min}$ vs q with slope 0.65557(7); (c) Overlap of the curves shown in (a) onto a single and universal plot after the transformation $e_{\min} \to e_{\min}/a^{0.65557}$.

was obtained analysing the crossover n_x as function of the control parameters. We discussed the behaviour of the energy of the particle as a function of the parameter r, which has a different behaviour, showing plateaus with constant energies. It was noticed that a region with strong stickiness do not let the diffusion of the particles to be observed, therefore trapping the particles for long enough time in some regions. Regarding function f_4, we have shown that the position of the minimum of the lowest invariant spanning curve is scaling invariant with respect to q.

Acknowledgements

D.R.C. acknowledges Brazilian agency FAPESP. E.D.L. thanks to CNPq, FUNDUNESP and FAPESP, Brazilian agencies. This research was supported by resources supplied by the Center for Scientific Computing (NCC/GridUNESP) of the São Paulo State University (UNESP).

References

[1] M. Buttiker, R. Landauer, Phys. Rev. Lett. 49 (1982) 1739.
[2] O. Farago, Y. Kantor, Physica A 249 (1998) 151.
[3] J.L. Mateos, J.V. José, Physica A 257 (1998) 434.
[4] J.L. Mateos, Phys. Lett. A 256 (1999) 113.
[5] M. Leng, C.S. Lent, Phys. Rev. Lett. 71 (1993) 137.
[6] L.P. Kouwenhoven, F.W.J. Hekking, B.J. van Wees, C.J.P.M. Harmans, C.E. Timmering, C.T. Foxon, Phys. Rev. Lett. 65 (1990) 361.
[7] L.P. Kouwenhoven, S. Jauhar, J. Orenstein, P.L. McEun, Y. Nagamune, J. Motohisa, H. Sakaki, Phys. Rev. Lett. 73 (1994) 3443.
[8] P.S.S. Guimarães, B.J. Keay, J.P. Kaminski, S.J. Allen Jr., P.F. Hopkins, A.C. Gossard, L.T. Florez, J.P. Harbison, Phys. Rev. Lett. 70 (1993) 3792.
[9] V. Berdichevsky, M. Gitterman, Phys. Rev. E 59 (1999) R9.
[10] V. Berdichevsky, M. Gitterman, J. Phys. A: Math. Gen. 29 (1996) L447.
[11] V. Berdichevsky, M. Gitterman, Phys. Rev. E 53 (1996) 1250.
[12] V. Berdichevsky, M. Gitterman, J. Phys. A: Math. Gen. 29 (1996) 1567.
[13] S. Upadhyay, J. Phys. A: Math. Gen. 24 (1991) L1293.
[14] V. Berdichevsky, M. Gitterman, Phys. Rev. E 60 (1999) 7562.

[15] Y. Zolotaryuk, V.N Ermakov, P.L. Christiansen, J. Phys. A: Math. Gen. 37 (2004) 6043.
[16] W. Cai, T.F. Zheng, P. Hu, B. Yudanin, M. Lax, Phys. Rev. Lett. 63 (1989) 418.
[17] J. Iwaniszewski, Phys. Rev. E 68 (2003) 027105.
[18] B. Cui, L.C. Wang, X.X. Yi, Phys. Rev. A 82 (2010) 062105.
[19] M. Bagheri, M. Poot, M. Li, W.P.H. Pernice, H.X. Tang, Nat. Nanotechnol. 6 (2011) 726.
[20] Y.-X. Li, Y. Xu, Chin. Phys. B 19 (2010) 057202.
[21] Q.T. Xie, J. Phys. A: Math. Theor. 45 (2012) 175302.
[22] D.W. Zhang, L.B. Fu, Z.D. Wang, S.L. Zhu, Phys. Rev. A 85 (2012) 043609.
[23] H. Cao, L.B. Fu, Eur. Phys. J. D 66 (2012) 97.
[24] V.M. Rozenbaum, I.V. Shapochkina, Phys. Rev. E 84 (2011) 051101.
[25] B. Dybiec, J. Chem. Phys. 133 (2010) 244114.
[26] G.A. Luna-Acosta, G. Orellana-Rivadeneyra, A. Mendoza-Galván, C. Jung, Chaos Solitons Fract. 12 (2001) 349.
[27] E.D. Leonel, J.K.L. da Silva, Physica A 323 (2003) 181.
[28] J. Wu, et al., Phys. Lett. A 262 (1999) 245.
[29] E.D. Leonel, J.A. Oliveira, F. Saif, J. Phys. A: Math. Theor. 44 (2011) 302001.